

Finite-temperature behavior of small silicon and tin clusters: An *ab initio* molecular dynamics study

Sailaja Krishnamurty, Kavita Joshi, and D. G. Kanhere

Department of Physics and Centre for Modeling and Simulation, University of Pune, Ganeshkhind, Pune-411 007, India

S. A. Blundell

*Département de Recherche Fondamentale sur la Matière Condensée, CEA-Grenoble/DSM, 17 rue des Martyrs,
F-38054 Grenoble Cedex 9, France*

(Received 18 June 2005; revised manuscript received 8 November 2005; published 18 January 2006)

The finite-temperature behavior of small silicon and tin clusters (Si_{10} , Si_{15} , Si_{20} , Sn_{10} , and Sn_{20}) is studied using isokinetic Born-Oppenheimer molecular dynamics. We find that the low-lying structures for all the clusters are built upon a highly stable tricapped trigonal prism unit which is seen to play a crucial role in the finite-temperature behavior. The thermodynamics of small tin clusters is revisited in light of the recent experiments on tin clusters of sizes 18–21 [G. A. Breaux *et al.*, Phys. Rev. B, **71**, 073410 (2005)]. Our calculated heat capacities for Si_{10} , Sn_{10} , and Si_{15} show main peaks around 2300, 2200, and 1400 K, respectively. The finite-temperature behavior of Si_{10} and Sn_{10} is dominated by isomerization and it is rather difficult to discern their melting temperatures. On the other hand, Si_{15} does show a liquidlike behavior over a short temperature range, which is followed by fragmentation observed around 1800 K. The finite-temperature behavior of Si_{20} and Sn_{20} shows that these clusters do not melt but fragment around 1200 and 650 K, respectively.

DOI: [10.1103/PhysRevB.73.045419](https://doi.org/10.1103/PhysRevB.73.045419)

PACS number(s): 61.46.Bc, 36.40.Cg, 36.40.Ei

I. INTRODUCTION

The finite-temperature behavior of small clusters is of great interest due to the recent exciting calorimetric measurements carried out on clusters of sodium, tin, gallium and aluminum.^{1–5} The experiments on tin and gallium clusters with sizes between 10–50 atoms reveal many interesting features. For example, contrary to the standard paradigm it has been shown that these clusters can have higher-than-bulk melting temperatures.^{2,3} Further, the addition of a single atom is seen to change the specific-heat curve dramatically.⁴ These experiments have motivated many researchers to simulate the finite-temperature behavior of small clusters.^{6–13}

In the present work, we study the finite-temperature behavior of small silicon and tin clusters. Silicon clusters are of potential relevance to the nanoelectronics industry and hence remain the subject of many experimental as well as theoretical studies.^{14–30} A majority of the theoretical studies are devoted to the investigation of low-energy equilibrium geometries of small silicon clusters. These studies are motivated by the experimental findings that Si clusters undergo a structural transition from prolate to spherical shapes in the size range 22–34.^{14,20} To date, the global minima of silicon clusters with sizes $n < 24$ have been characterized by employing various unbiased search mechanisms such as genetic algorithms, the single-parent evolution algorithm, and “big bang” optimization.^{16,22,26}

A number of experimental investigations using surface-induced dissociation techniques revealed that the fragmentation behavior is common within the clusters of semiconducting group IV elements.^{31,32} Many of the studies on silicon clusters indicate the preference of a fragmentation pathway over an evaporation process.^{15,33} Specifically, these studies predict that clusters with sizes 6–10 are the most abundant

fragments and these are referred to as magic fragments.^{21,34} Although it is speculated that silicon clusters up to sizes of 70 will undergo fragmentation rather than evaporation,¹⁵ it is not yet clear whether the clusters undergo the traditional solidlike-to-liquidlike transition before fragmenting or whether they fragment without melting as reported recently in the case of tin clusters.³⁵ Hence, we report detailed thermodynamic simulations on Si_n clusters with sizes $n=10, 15$, and 20. These simulations have been carried out using density-functional theory (DFT) within the generalized gradient approximation (GGA). The total simulation time for each cluster is at least 2 ns. Our studies indicate that the finite-temperature behavior of Si_{10} is dominated by isomerization and it is rather difficult to identify a region corresponding to a solidlike-to-liquidlike transition. However, the cluster clearly fragments around 2800 K. Si_{15} , on the other hand, does exhibit a liquidlike phase over a short temperature range before fragmenting around 1800 K. Si_{20} does not melt but fragments around 1200 K.

Both silicon and tin are group IV elements and it is interesting to note some peculiarities of this group. Carbon, the first element, is a nonmetal with a high-energy gap between the valence and conduction bands (around 5.5 eV), whereas silicon and germanium are semiconductors at room temperature. Tin and lead are metals at room temperature, but tin undergoes a structural phase transition and transforms into a semiconductor below 286 K. Contrary to the situation in the bulk, the low-lying structures of small tin clusters ($n < 25$) resemble greatly those of small silicon and germanium clusters.^{6,36} Interestingly, Si, Ge, and Sn clusters with sizes greater than 9 are built on stable tricapped trigonal prism (TTP) units, which as we shall see plays a crucial role in determining the finite-temperature behavior of these clusters. However, in contrast to silicon clusters, tin clusters undergo

a shape rearrangement from prolate (stacked TTP units) to a more compact spherical shape over a rather broad size range (35–65 atom clusters).³⁶ Ionic mobility experiments on small tin clusters (10–30 atoms) indicate that these clusters do not melt at least up to 50 K above the bulk melting temperature.² This conclusion is based on the argument that the onset of a liquid phase is characterized by a change in shape from prolate to spherical, and hence enhances ionic mobilities in the liquidlike region.² Density functional simulations supported these findings and showed that the melting temperatures of small tin clusters are indeed at least 1000 K higher than that of T_m (bulk).^{6,8,9,12} Our previous calculations, within the local density approximation (LDA), showed that Sn_{10} has a substantially higher melting temperature (2300 K), while Sn_{20} is in a liquidlike phase after 1200 K.^{8,9} However, the recent experiments on Sn_{18}^+ , Sn_{19}^+ , Sn_{20}^+ and Sn_{21}^+ demonstrated that these clusters do not melt but sublime around 650 K.³⁵ In view of these findings we simulate here the thermodynamics of the clusters Sn_{10} and Sn_{20} using both the LDA and GGA exchange-correlation functionals. In addition, the present simulations extend over a much longer time scale, at least 90 ps per temperature as compared to our earlier simulations of 40 ps per temperature.^{8,9} Our studies confirm the fragmentation observed experimentally and bring out similarities between small tin and silicon clusters in terms of their structure and dynamics.

In what follows, we present computational details in Sec. II. The thermodynamics of both silicon and tin clusters along with some error analysis is presented in Sec. III. We discuss various issues concerning the structure and dynamics of all the clusters in the same section. We conclude our paper in Sec. IV.

II. COMPUTATIONAL DETAILS

All the thermodynamic simulations are performed using Born-Oppenheimer molecular dynamics based on the Kohn-Sham formulation of DFT.³⁷ We have used ultrasoft pseudopotentials³⁸ within the GGA, as implemented in the VASP package.³⁹ The thermodynamic behavior of tin clusters is also studied within the LDA. For Si, we use $3s^2$ and $3p^2$ electrons as valence, whereas for Sn we use $5s^2$ and $5p^2$ electrons as valence, taking the d electrons as a part of the ionic core. Energy cutoffs of 13.84 and 9.77 Ry are used for the plane-wave expansion of Si and Sn wave functions, respectively, with a convergence in the total energy of the order of 10^{-4} eV. Cubic supercells of length 15, 18, and 22 Å are used for 10-, 15- and 20-atom clusters, respectively. We have ensured that the results are converged with respect to a further increase in E_{cut} and in the size of the simulation box.

The ground state and the other equilibrium structures of all the clusters are found by optimizing several structures chosen from a high-temperature simulation. Typically we have chosen about 100 geometries as our initial configurations for optimization. We analyze the nature of the bonding of the ground state and the other low-energy isomers using the electron localization function (ELF).⁴⁰ This function has been found useful for characterizing the strength of the bond especially in the case of covalently bonded systems.⁸ The

ELF is normalized between zero and unity; a value of 1 represents a perfect localization of electron density, while the value for a delocalized electron density is 0.5. Typically, the existence of an isosurface along the bonding region between two atoms at a high ELF value, say at 0.7 or greater, signifies a localized bond in that region.

Turning to the finite-temperature properties of the clusters, we would like to note that while performing experiments the cluster is maintained at a particular temperature with the help of a heat bath. Molecular dynamics (MD) simulations of a cluster within a canonical ensemble thus closely resemble the experimental conditions. Therefore in the present work the finite-temperature behavior is studied by sampling the ionic phase space of clusters using an isokinetic MD, which yields a canonical ensemble of cluster potential energies.^{41,42} However, we would like to comment that microcanonical heat-capacity curves may also be extracted from our simulations, yielding qualitatively similar results to the canonical curves presented here.⁹ Further, there are a number of different ways of simulating the canonical ensemble. One way is to couple a thermostat to the cluster, as in the Nosé-Hoover method.⁴¹ In our current study we use the more straightforward approach of holding the kinetic energy constant by scaling the velocities after every 5 MD steps. We have checked that the scaling of velocities after every 5 MD steps results in an appropriate balance between relaxation of the cluster and maintaining the desired temperature. This was done by scaling the velocities after every 3, 4, 5, 7, and 10 steps and verifying the velocity distribution at that temperature.

It should also be noted that the velocity-scaling algorithm may be shown⁴¹ to be an approximation to the isokinetic scheme of Evans and Morriss,⁴² in which while the kinetic energy is constant, the potential energy is sampled according to a canonical distribution, as is required as input for a multiple-histogram (MH) analysis⁴³ to compute the heat capacities. To demonstrate that the potential-energy distribution (PED) obtained by velocity scaling and via a Nosé thermostat is statistically similar, we show histograms of the PED for two temperatures in Fig. 1. The figure shows that the PED obtained using both the methods completely overlap, thereby validating the use of velocity scaling in our simulations.

Following the finite-temperature study, the ionic heat capacity of each cluster is computed using the multiple-histogram method.^{43,44} The computation of the heat capacity using the MH technique is sensitive to the number of temperatures at which the thermodynamic behavior of the cluster is simulated. The range and the number of temperatures must be chosen to ensure an adequate overlap of PED's. Further aspects of the MH technique and computation of the heat capacity are given in Sec. of III A.

In the current study we have chosen 22 different temperatures in the range 100 K–3000 K for the case of Si_{10} and Sn_{10} so as to ensure sufficient overlap the PED between two successive temperatures. In the case of Si_{15} and Si_{20} clusters, we split the temperature range 100 K–1800 K into 14 different temperatures. To verify the experimentally reported fragmentation we have carried out a finite-temperature study of Sn_{20} at only at few temperatures, namely, 200, 350, 500,

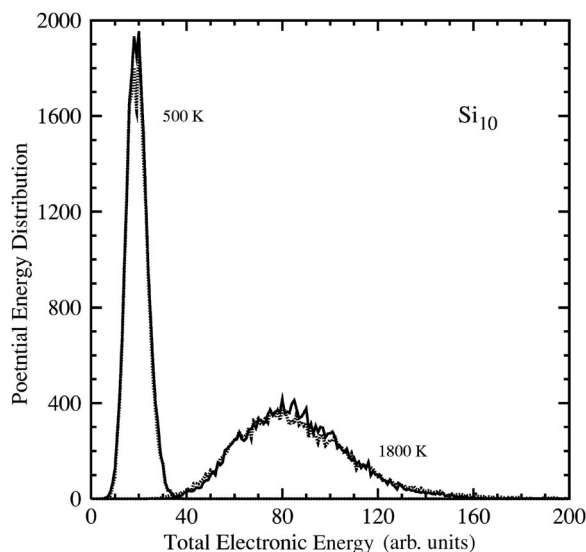


FIG. 1. Potential-energy distribution for Si_{10} using velocity scaling (—) and a Nosé-Hoover thermostat (...) at 500 and 1800 K for a time period of 60 ps.

and 650 K. We have also investigated thermodynamics of Sn clusters within the LDA to understand the influence of the exchange and correlation functional on the reported fragmentation behavior.

The classical ionic density of states $\Omega(E)$ of the cluster, or equivalently the classical ionic entropy $S(E) = k_B \ln \Omega(E)$, are extracted from the simulation data following the MH technique. With $S(E)$ in hand, one can evaluate thermodynamic averages in a variety of ensembles. We focus in this work on the ionic specific heat and the caloric curve. In the canonical ensemble, the specific heat is defined as usual by $C(T) = \partial U(T) / \partial T$, where $U(T) = \int E p(E, T) dE$ is the average total energy, and where the probability of observing an energy E at a temperature T is given by the Gibbs distribution $p(E, T) = \Omega(E) \exp(-E/k_B T) / Z(T)$, with $Z(T)$ the normalizing canonical partition function.

Various other thermodynamic indicators such as the mean-square ionic displacement (MSD) and the root-mean-square bond-length fluctuation (δ_{rms}) are computed. For the sake of completeness we briefly discuss these parameters. The parameter δ_{rms} is a measure of the fluctuations in the bond lengths averaged over all atoms and over the total time span. It is defined as

$$\delta_{\text{rms}} = \frac{2}{N(N-1)} \sum_{i>j} \frac{(\langle r_{ij}^2 \rangle_t - \langle r_{ij} \rangle_t^2)^{1/2}}{\langle r_{ij} \rangle_t}, \quad (1)$$

where N is the number of atoms in the system, r_{ij} is the distance between atoms i and j , and $\langle \rangle_t$ denotes a time average over the entire trajectory. The MSD is another widely used parameter for analyzing a solidlike-to-liquidlike transition and is defined as

$$\langle \mathbf{r}^2(t) \rangle = \frac{1}{NM} \sum_{m=1}^M \sum_{l=1}^N [\mathbf{R}_l(t_{0m} + t) - \mathbf{R}_l(t_{0m})]^2, \quad (2)$$

where N is the number of atoms in the system and \mathbf{R}_l is the position of the l th atom. Here we average over M different

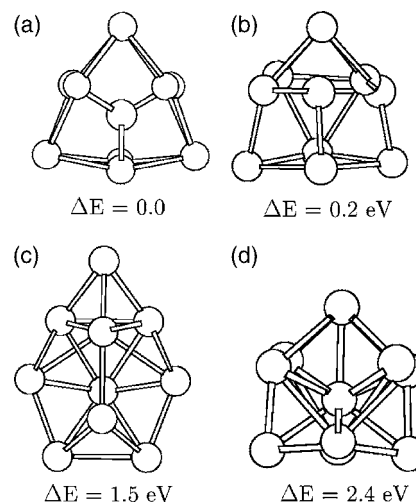


FIG. 2. The ground state and some of the representative isomers of Si_{10} . ΔE is the difference in total energy with respect to the ground-state energy.

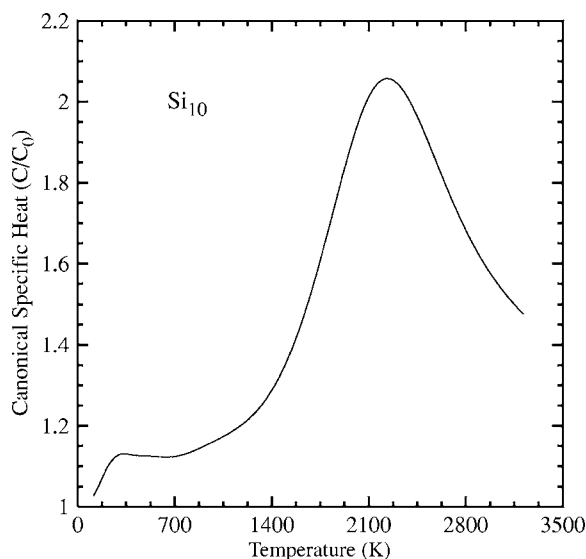
time origins t_{0m} spanning the entire trajectory. The interval between the consecutive t_{0m} for the average was taken to be about 0.0125 ps. The MSD indicates the displacement of atoms in the cluster as a function of time. In the solidlike region, all atoms perform oscillatory motion about fixed points resulting in a negligible mean displacement of individual atoms from their equilibrium positions. (We hold the total angular momentum of the cluster to zero, suppressing cluster rotation.) In a liquidlike state, on the other hand, atoms diffuse throughout the cluster and the MSD eventually reaches a saturated value of the order of the square of the cluster radius. More technical details concerning the extraction of thermodynamics averages, indicators, and computation of the specific-heat curve can be found in previous work.⁴⁴

III. RESULTS AND DISCUSSION

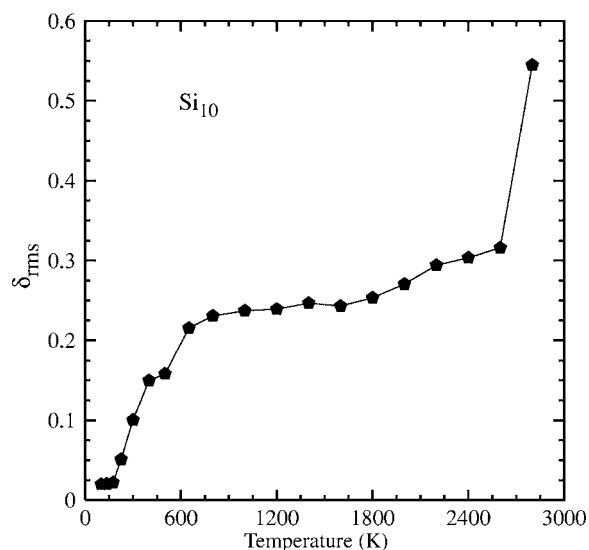
A. Thermodynamics of silicon clusters

We begin with a discussion of the zero-temperature properties of Si_{10} . The ground-state structure and other low-lying isomers are shown in Fig. 2. The ground state of Si_{10} is a tetra-capped trigonal prism similar to that of Sn_{10} (Ref. 18) and is consistent with the one reported earlier.⁴⁵ This is a very stable structure with C_{3v} symmetry. It may be noted with some interest that the ground state and the first high-energy configuration (higher by 0.2 eV) contain one TTP unit whereas all other configurations contain no TTP unit. This is the reason for the significant energy difference of ~ 1.3 eV between the first two equilibrium structures and the remaining higher-energy configurations. We also note that in the ground state geometry all the atoms except the one capping the triangular face of the trigonal prism have at least fourfold coordination. We have analyzed the nature of the bonding using the ELF, which shows the expected covalent bonding among all the silicon atoms (figure not shown).

Turning to the analysis of the finite-temperature behavior of the cluster, we show the calculated heat capacity for Si_{10}

FIG. 3. Normalized canonical heat capacity of Si_{10} .

in Fig. 3. The salient features of the curve are a main peak around 2200 K and presence of a weak shoulder from 350 to 1000 K. Generally, the peak in the heat capacity is associated with the solidlike-to-liquidlike transition. However, a detailed analysis of ionic trajectories at various temperatures, along with δ_{rms} and the MSD, indicates that this peak is, in fact, associated with the fragmentation observed around 2800 K. The analysis of ionic motion at various temperatures reveals several additional features. For example, the shoulder at 350 K arises from a structural transition of the cluster from the ground state to the first isomer and then back to the ground state. This process is triggered by the attempt of the tricoordinated atom (the atom capping the triangular face of the trigonal prism) to acquire a fourth neighbor. The isomerization seen around 350 K is quite similar to the one observed in the case of Sn_{10} (Ref. 8) and leads finally to the exchange of positions of at least three atoms (the cap on triangular face, one on a rectangular face, and an atom from the trigonal prism). This isomerization process continues with increasing frequency until 1400 K and results in the overall diffusion of atoms throughout the cluster, but without changing the geometry significantly. It is only around 1600 K and beyond that the structures corresponding to other isomers are observed. Thus the rise in the heat capacity observed after 1400 K is associated with the destruction of the TTP unit and the occurrence of other isomers. At much higher temperatures, around 2300 K and above, we observe several high-energy configurations which can be thought of as two weakly bonded clusters of smaller sizes. The signature of nascent fragmentation is observed around 2300 K, where Si_{10} can be considered as weakly interacting $\text{Si}_7 + \text{Si}_3$ fragments or $\text{Si}_6 + \text{Si}_4$ fragments for about 5% of the total simulation time. The fragmentation process dominates with increasing temperature and we observe $\text{Si}_3 + \text{Si}_7$ fragments for about 70% of the simulation time at 2600 K. In the simulation we performed, the cluster eventually fragmented around 2800 K into Si_7 and Si_3 . We have not attempted to obtain the statistical distribution of final fragments; it is possible that one would also find Si_6 and Si_4 or other final frag-

FIG. 4. Root-mean-square bond-length fluctuation δ_{rms} [Eq. (1)] for Si_{10} .

ments if the simulations were repeated many times.

In Fig. 4 we present δ_{rms} [Eq. (1)] for Si_{10} . It is clearly seen that δ_{rms} is characterized by two sharp steps, the first one from 175–650 K and another at 2800 K. According to the bulk Lindemann criterion, a value of δ_{rms} greater than 0.1 is indicative of transition from a solidlike state to a liquidlike state. In the present case, δ_{rms} reaches a value of 0.2 at 650 K. This is due to the fact that the transition from the ground state to the first isomer and back, discussed earlier, results in a net diffusion of atoms throughout the cluster and thereby saturates the value of δ_{rms} . The value of δ_{rms} is almost constant for the next 1000 K (i.e., up to 1600 K). Above 1600 K, coincident with the destruction of the TTP unit, δ_{rms} experiences a gradual and slow rise until 2600 K. This gradual rise ends with a sharp jump at 2800 K due to the observed fragmentation.

Next we analyze the radial distribution function defined as the average number of atoms within the region r and $r+dr$ from the center of mass, which is shown in Fig. 5. In symmetric systems such as Si_{10} , a sharp peak in the radial distribution function indicates the existence of geometric shells within the cluster. At low temperatures this shell structure is retained as observed for 100 K [shown in Fig. 5(a)]. Let us note that the first two peaks correspond to the two faces of the trigonal prism, the third peak corresponds to the caps on the rectangular surfaces, and the last one is due to the cap on the triangular face. With increasing temperature the peaks begin to merge, indicating the exchange of atoms between the various shells. Around 650 K, the four peaks merge into two and the radial distribution of atoms remains nearly identical until 1400 K. Above 1600 K, the plot indicates the absence of order in the arrangement of the atoms. The peak gets broader at higher temperatures and around 2300 K the radial distribution function is seen as a broad curve.

To summarize, the heat capacity shows a main peak around 2300 K which is attributed to the fragmentation of the cluster. The cluster undergoes characteristic isomerization for a very broad range of temperatures between 650 K

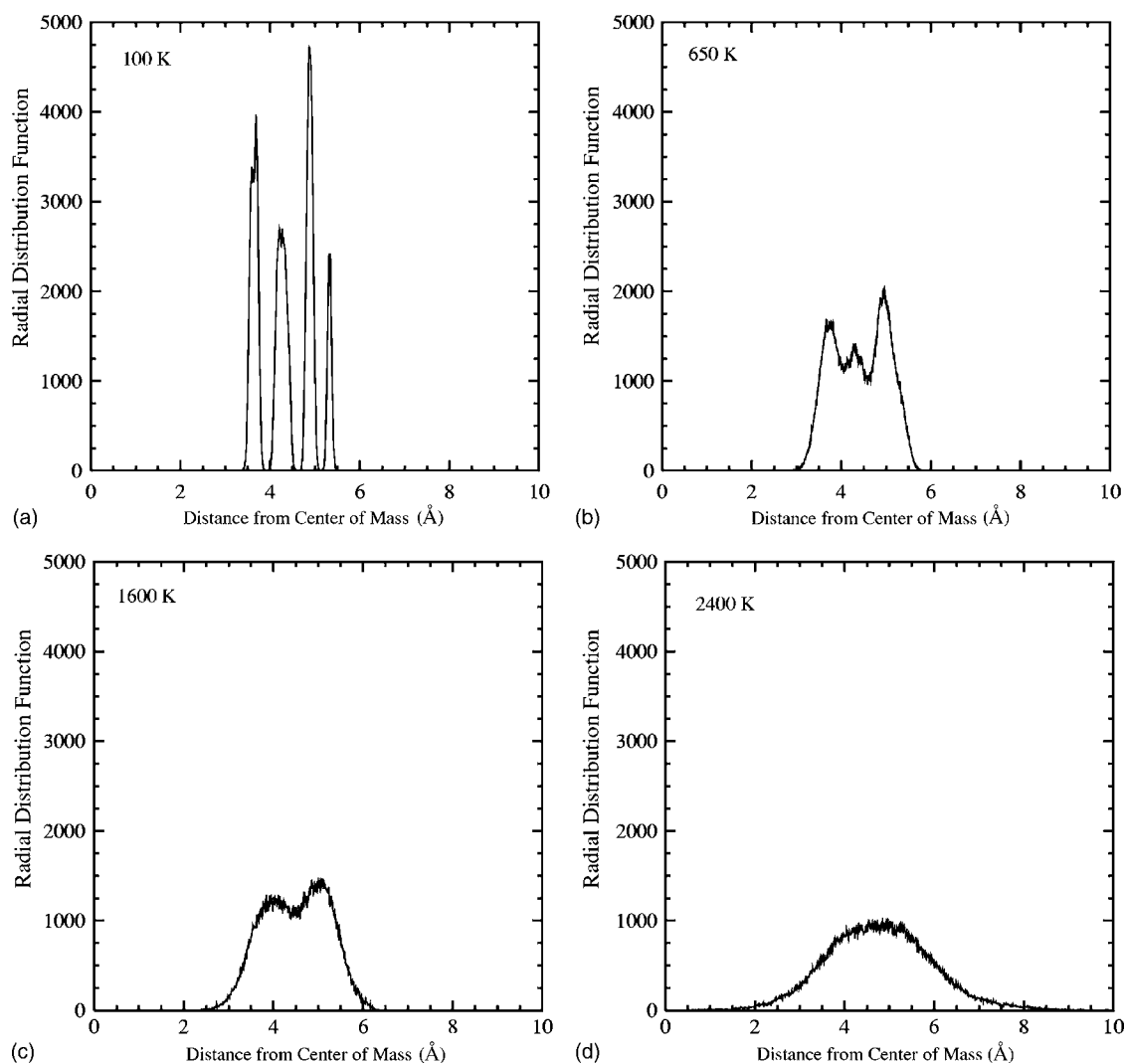


FIG. 5. Atomic distribution from the center of mass for Si_{10} .

and 1400 K where it retains the memory of the ground state but undergoes a rearrangement process resulting in the net diffusion of the atoms throughout the cluster. Thus the finite-temperature behavior of very small clusters such as Si_{10} is dominated by isomerization. The solidlike-to-liquidlike transition is continuous and it is rather difficult to discern a transition region.

It may be recalled that finite-temperature behavior is sensitive to the size of the cluster⁴ and hence it will be interesting to investigate silicon clusters with different sizes. We therefore extend our finite-temperature investigations to Si_{15} and Si_{20} . Both these clusters have a TTP subunit in many of their low-lying isomers, which as we shall see plays a crucial role in their thermodynamics. We begin the discussion by analyzing the equilibrium structures of Si_{15} . We have obtained at least 30 different equilibrium structures out of which few relevant structures are shown in Fig. 6. The ground-state geometry of Si_{15} can be described as a tricapped trigonal prism fused with a tricapped trigonal antiprism [C_{3v} symmetry, Fig. 6(a)]. This is consistent with the low-energy configuration reported in DFT simulations²² and in coupled-cluster studies.²⁸ The first high-energy configuration consists

of two TTP units sharing a common triangular face, as shown in Fig. 6(b). This structure can be viewed as a serious distortion of the lower six-atom ring present below the TTP unit in the ground state. The first few isomers are built on the TTP unit of Si_9 , as shown in Figs. 6(b) and 6(c), whereas the isomers observed at higher temperatures can be thought of as a combination of two small silicon clusters, as seen in Fig. 6(d), and suggest probable pathways for fragmentation.

Turning to the finite-temperature behavior of Si_{15} , we show the ionic heat capacity in Fig. 7. The specific-heat curve shows a main peak around 1400 K and has two small features around 400 and 800 K. As we shall see later, the main peak is associated with the observed fragmentation of the cluster around 1800 K. A plausible explanation for the different features observed in the heat capacity can be obtained by examining the ionic motion of the cluster at various temperatures. Around 400 K, we observe an isomerization process similar to that of Si_{10} . The Si_{15} cluster undergoes a transition from the ground state to the first isomer and back to the ground state with 180° rotation. However, this transition does not involve the net diffusion of atoms and continues to occur with increasing frequency until 700 K. A further

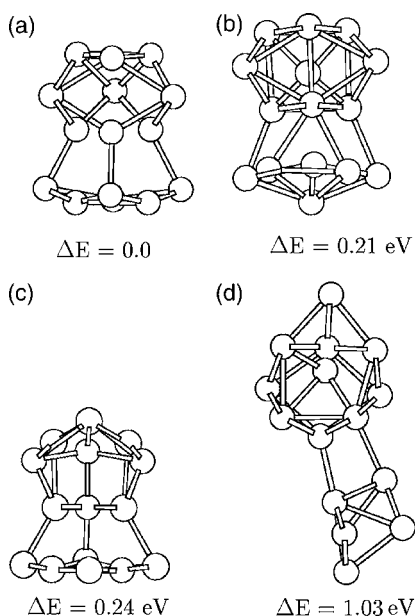


FIG. 6. The ground state and some of the representative isomers of Si_{15} . ΔE is the difference in total energy with respect to the ground-state energy.

rise in temperature then leads to several other isomerization processes, which result in a net diffusion of atoms throughout the cluster. This corresponds to the second shoulder seen in the specific-heat curve around 800 K (see Fig. 7). Around 1200 K, isomers corresponding to two small weakly interacting silicon clusters [Fig. 6(d)] are observed in the ionic motion, which provides a fragmentation pathway at higher temperatures. Thus the feature around 400 K is due to the isomerization and the small peak around 800 K is a “melt-like” peak, while the main peak around 1400 K is due to the fragmentation.

These observations are in agreement with the plot of δ_{rms} , shown in Fig. 8 for over 75 ps of simulation per temperature point. A nearly constant δ_{rms} at lower temperatures (below

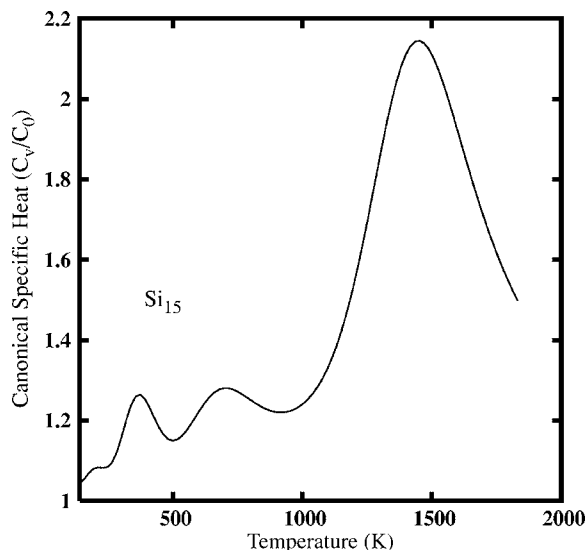


FIG. 7. Normalized canonical heat capacity of Si_{15} .

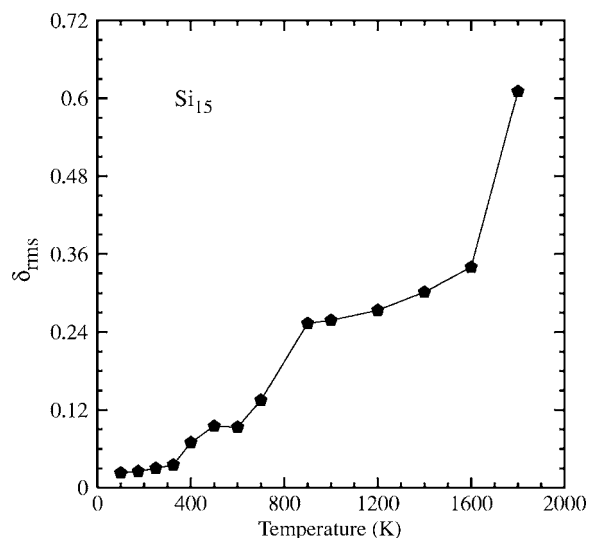


FIG. 8. Root-mean-square bond-length fluctuation δ_{rms} [Eq. (1)] for Si_{15} .

400 K) is indicative of purely vibrational motion. Above 400 K, δ_{rms} increases linearly due to the observed isomerization. The value of δ_{rms} saturates after 900 K showing a liquidlike state over a short temperature range. The sharp rise at 1800 K indicates fragmentation of the cluster at that temperature into Si_9 and Si_6 . These fragments are the most dominant fragments during our simulation, although we observe $\text{Si}_{10} + \text{Si}_5$ and $\text{Si}_8 + \text{Si}_7$ for less than 10% of the total simulation time.

It is interesting to compare the finite-temperature behavior of Si_{15} and Si_{10} . Although both clusters fragment, Si_{15} dissociates at a considerably lower temperature (1800 K) than Si_{10} (2600 K). The higher fragmentation temperature for Si_{10} can be attributed to the fact that it involves the breaking of a strongly bonded TTP unit, while in the case of Si_{15} the fragmentation is associated with the separation of the TTP unit from the rest of the cluster.

Now we present our results for Si_{20} . First we note a few interesting changes in the trends of the ground-state geometry of small Si clusters. It is well known that the ground state of silicon clusters with sizes 9–17 are built upon a TTP unit, whereas from 18 onward the TTP unit is absent in the ground state but is observed in most of the low-lying configurations.^{28,29} However, the ground state of these systems continues to be a prolate configuration. Another interesting observation is the existence of nonprolate structures with a similar energy to that of the prolate structures. It is expected that these clusters will also fragment, as in the case of Si_{10} and Si_{15} . However, the presence of low-lying spherical configurations opens up an interesting question as to whether these clusters will undergo a prolate-to-spherical shape transformation before fragmenting. This prolate-to-spherical transformation is considered as a signature of melting.² This has motivated us to analyze the finite-temperature behavior of Si_{20} .

The ground-state geometry and the various high-lying configurations of Si_{20} have been well studied in earlier works.²⁹ It may be noted that the ground state of Si_{20} is a

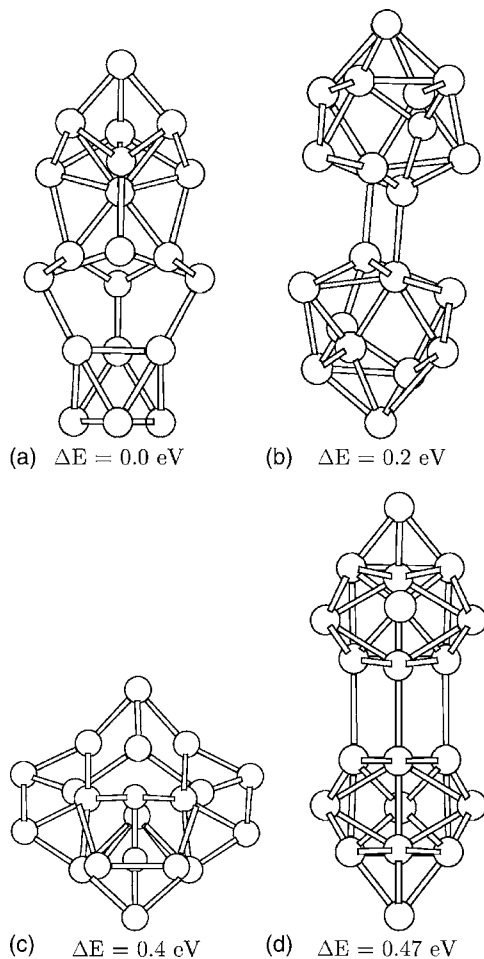


FIG. 9. The ground state and some of the representative isomers of Si_{20} . ΔE is the difference in total energy with respect to the ground-state energy.

prolate structure and is composed of three units: a so-called magic number cluster Si_6 , a hexagonal chair unit in the middle, and a unit corresponding to a low-energy isomer of Si_8 . The first high-energy configuration [see Fig. 9(b)] consists of two distinct TTP units, whereas the second one is a nonprolate spherical structure [see Fig. 9(c)]. The fourth equilibrium structure that we have shown in the figure [Fig. 9(d)] has two weakly bonded Si_{10} units (bond lengths of 2.7 \AA as compared to the normal Si–Si covalent bond length of 2.34 \AA). As we shall see, the cluster fragments via this isomer. All the equilibrium structures shown here are consistent with earlier reports.^{26,21} We have examined the nature of the bonding of the ground state and other isomers using the ELF and found it to be covalent.

We now discuss the finite-temperature behavior of Si_{20} . The ionic motion of the cluster shows that the atoms vibrate about their mean positions until 800 K. Around 1000 K, the cluster transforms from the ground state to the first high-energy configuration with two distinct Si_{10} units [Fig. 9(b)] and eventually fragments into two Si_{10} units around 1200 K. This is reflected in the plot of δ_{rms} shown in Fig. 10, where the fragmentation is evident from the sharp rise around 1200 K.

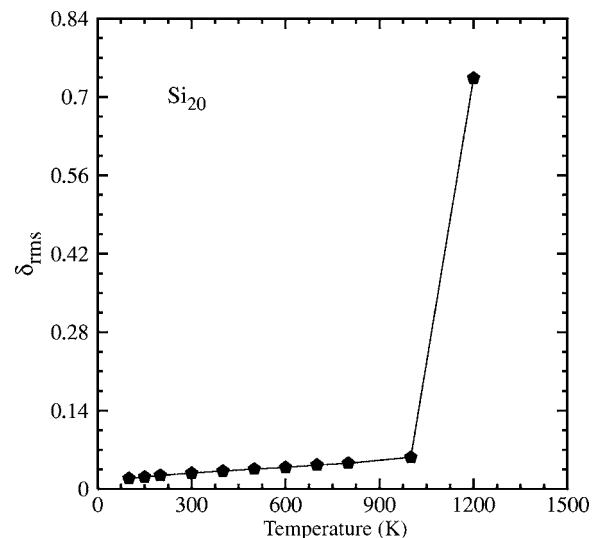


FIG. 10. Root-mean-square bond-length fluctuation δ_{rms} [Eq. (1)] for Si_{20} .

To investigate whether the observed fragmentation is sensitive to the starting configurations, we have repeated the thermodynamics of Si_{20} with a spherical configuration [Fig. 9(c)] as a starting geometry. It is seen that even in this case the cluster fragments around 1200 K and the fragmentation channel involves the isomer with two TTP units [Fig. 9(d)]. Thus the observed fragmentation is quite robust and independent of the starting configuration. However, the fragmentation behavior of the cluster is sensitive to the rate of heating of the cluster. To demonstrate this we present results obtained on Si_{20} clusters using different rates of heating. In all the above simulations, the cluster is heated to a particular temperature from the previous temperature at a rate of 1 K per 30 fs and then maintained at that temperature for next 30 ps. This is used as a starting point for heating the cluster to the next temperature. We observed the fragmentation after maintaining the cluster at 1200 K for at least 60 ps. On the other hand, we have observed a completely different behavior of the cluster when heated directly from 1200 to 1600 K at a much faster rate of 1 K per 3 fs without thermalizing it around 1200 K. We notice that in this case the cluster does not fragment and trajectories at this temperature reveal that the two TTP structures merge; a highly diffusive motion of atoms within the cluster is then observed, thus signaling the presence of a liquidlike state. Thus the cluster appears to bypass the fragmentation step. The value of δ_{rms} at this temperature is around 0.35. This liquidlike state continues to be observed as the temperature is increased to 1800 K. We note further that the liquidlike state, once formed, is sustained at both the temperatures for a time period of 100 ps.

Thus it turns out that fast heating pumps enough kinetic energy in the cluster leading to shorter inter-TTP bond distances. Consequently, the two TTP units begin to fuse leading to the high-energy configurations (containing no TTP units) as shown in Fig. 11. Further analysis of the ionic motion at 1600 K shows that the cluster oscillates between prolate configurations (70% of simulation time) and nonprolate (nearly spherical) configurations (30% of simulation time).

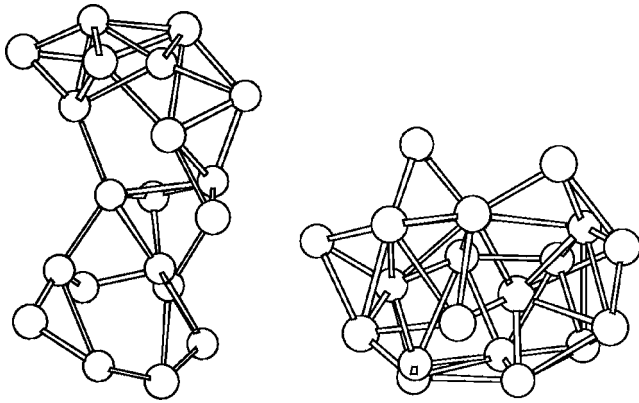


FIG. 11. Prolate and spherical configurations of Si_{20} around 1800 K.

As the temperature increases to 1800 K, the cluster spends more time in the nearly spherical configurations (60% of simulation time).

To summarize, the finite-temperature behavior of Si_{20} does not show any solidlike-to-liquidlike transition prior to fragmentation, unlike the cases of Si_{10} and Si_{15} . Further, the fragmentation occurs at much lower temperatures than for Si_{10} and Si_{15} . This lowering of the fragmentation temperature is due to the fact that the ground state and low-lying geometries of Si_{10} and Si_{15} clusters are built around a highly stable TTP unit, whereas the low-lying isomers of Si_{20} are composed of two weakly interacting TTP units. The lowering of the fragmentation temperature with increasing cluster size is in agreement with the experimentally reported dissociation energy barriers for Si_{20} (dissociation energy of the order of 1.2 eV), Si_{15} (2.2 eV), and Si_{10} (4.2 eV).¹⁵

B. Thermodynamics of tin clusters

The recent experimental results reveal that small tin clusters (with sizes 18–22) fragment (around 650 K) without undergoing a solidlike-to-liquidlike transition.³⁵ These observations are at variance with our earlier simulations.⁹ Therefore we have revisited the thermodynamics of tin clusters. In the present work we have extended our simulations over a much longer time scale of 90 ps per temperature as compared to 40 ps per temperature in the earlier work. In addition to the LDA simulations performed in our earlier work, we have also carried out 90 ps runs using the GGA exchange-correlation functionals. These improved simulations bring out two interesting points: (a) the necessity of longer simulation time scales (at least of the order of ~ 90 ps per temperature), and (b) the need for a nonlocal exchange-correlation functional (GGA) for an improved description of energetics and bonding, especially in the case of Sn_{20} .

As to the results obtained on the Sn_{10} cluster, it turns out that ground-state geometry and various other low-lying isomers are similar within LDA and GGA. Thus we would expect the finite-temperature behavior given by both approximations to be similar. Indeed, as expected the specific-heat curves computed from GGA and LDA calculations are nearly similar, having a slightly shifted main peak around 2200 K

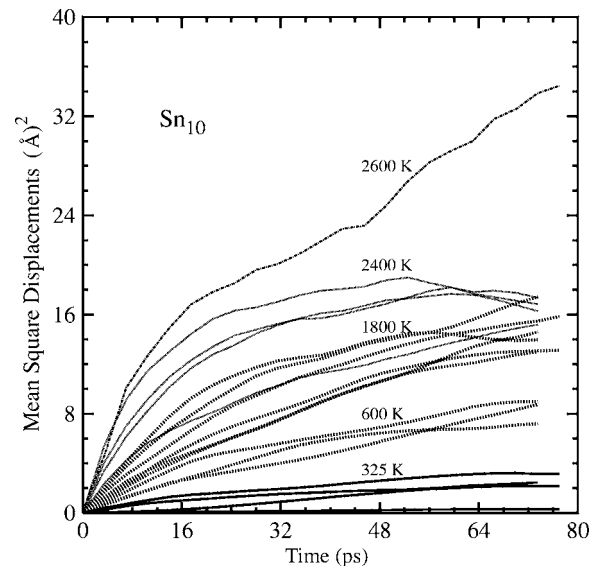


FIG. 12. Mean-square displacement of atoms in Å^2 as a function of time in ps [see Eq. (2)]. The top-most line corresponds to the mean-square displacement of atoms at 2600 K.

as compared to our earlier reported one at 2300 K (figure not shown).⁸ The only difference to be noted is the fragmentation of Sn_{10} observed at 2600 K in our extended simulations. However, this process is observed only after a time scale of about 60 ps. This will be evident from the average MSD's shown in Fig. 12. As expected, at lower temperatures the value of the MSD is small, indicating the vibrational motion of atoms, and it increases gradually with temperature. The sudden rise at 2600 K (after about 60 ps) is a signature of the observed fragmentation. We have explicitly verified this by visualizing the ionic motion, which shows that the cluster dissociates into Sn_6 and Sn_4 after a time period of 60 ps. We believe that this feature was present in a nascent form in our earlier simulations and was not seen explicitly. Quite clearly this feature is missing in our earlier reports due to the smaller simulation time scales (about 50 ps per temperature). It should be noted that the finite-temperature behavior of Sn_{10} is very similar to that of Si_{10} . This is, in fact, expected as the ground state and even the excited state configurations of Si_{10} and Sn_{10} are identical.

Now we present the finite-temperature properties of Sn_{20} . In our earlier paper,⁹ Sn_{20} melts around 1200 K, which is at variance with the recent experimental reports suggesting fragmentation around 650 K. In the present study we have found that within LDA, Sn_{20} fragments around 1200 K, whereas within GGA the fragmentation temperature is 650 K. Thus the GGA results are in perfect agreement with the recently reported experimental observations,³⁵ whereas the LDA results overestimate the fragmentation temperature. Analysis of bond lengths, binding energies, and dissociation energies within both approximations will throw light on the variation in the fragmentation temperature. In Table I we show the bond length, binding energy, and dissociation energy for the ground state within both the approximations.

It may be observed from Table I that: the inter-TTP bond lengths within LDA are shorter than those within GGA; the

TABLE I. Comparison between LDA and GGA results for Sn_{20} . The bond length indicates the average distance between two TTP units. The dissociation energy is the energy required to dissociate Sn_{20} into two Sn_{10} units. The binding energy reported below is per atom.

	LDA	GGA
Bond length (\AA)	3.18	3.34
Binding energy (eV)	4.04	3.57
Dissociation energy (eV)	0.98	0.51

binding energy within LDA is higher than that within GGA; and the dissociation energy of Sn_{20} within LDA is twice than that within GGA which is consistent with the observed fragmentation temperatures. This indicates that within LDA the TTP units are more strongly bonded than within GGA, which yields a higher fragmentation temperature.

The failure to detect the fragmentation behavior in our earlier reports is attributed to a combination of the following reasons: (a) the smaller simulation time scales in our earlier simulations (about 50 ps per temperature), (b) a faster heating rate, and (c) use of LDA functional in our earlier reports. As already mentioned,⁹ the ground state of the Sn_{20} cluster has an inhomogeneous bond-strength distribution. While the bonds within intra-TTP atoms are strongly covalent in nature, inter-TTP atoms are connected through weak covalent bonds as seen from Table I. The LDA approximation was unable to distinguish these differences leading to an overestimation of binding energies between the two TTP units. Hence, the Sn_{20} cluster did not fragment on the small simulation times scales reported earlier. By contrast, the Sn_{10} cluster has all its atoms connected with similar bond strengths, resulting in a more accurate finite-temperature behavior within the LDA approximation.

C. Error analysis

We conclude our discussion with a note on error analysis. We have studied the finite-temperature behavior of clusters using density-functional-based molecular dynamics within the plane-wave approximation. These simulations are subject to numerical errors due to the finite energy cutoff, the size of the simulation box, and the grid spacing. We have checked that the total energy and the forces are converged with respect to further improvement in the above parameters. Apart from these, another important source of error is the limited statistics for calculating finite-temperature properties. It may be noted that the *ab initio* nature of the method puts serious restrictions on the simulation times. The quality of our data can be accessed by examining the convergence of a typical parameter such as the root-mean-square bond-length fluctuation (δ_{rms}). In Fig. 13 we show δ_{rms} averaged over 30, 60, and 75 ps for Si_{15} . In each of these cases the thermalization time is at least 30 ps. It is quite evident from the figure that, although 30 ps are sufficient for low temperatures, we need more statistics in the transition region and above. It can be seen from the figure that δ_{rms} calculated for 60 and 75 ps are fairly well converged.

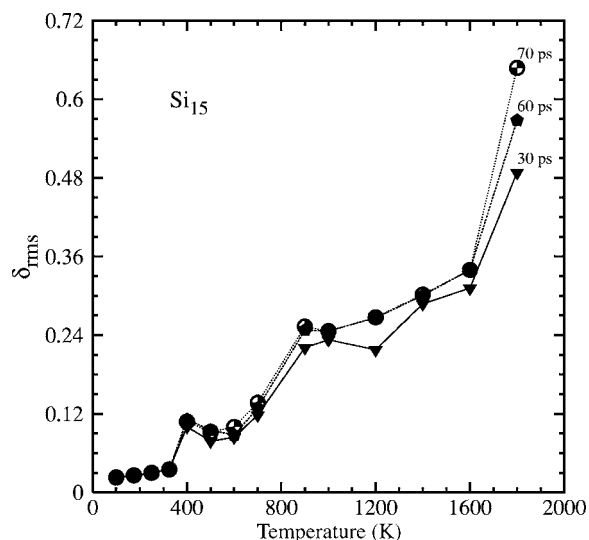


FIG. 13. Root-mean-square bond-length fluctuation δ_{rms} for Si_{15} comparing averages over 30 ps data, 60 ps data, and 75 ps data.

Next we compute the specific-heat curve using the MH technique from the simulated trajectories. The heat capacities depend crucially on the quality of the histograms and the number of temperatures used in the calculation. Since the method extracts the total density of states by sampling PED's at several temperatures, the choice and number of temperatures is crucial. The PEDs (histograms) for two successive temperatures need to have an appreciable overlap. To demonstrate this point we present the heat capacity of Si_{15} computed with two different sets of temperatures in Fig. 14. The heat-capacity curve (a) in Fig. 14 is computed from 9 different temperatures, as compared to the heat-capacity curve (b), which is computed from 14 different temperatures. Quite clearly the lower temperature features are not represented properly in curve (b) owing to an inadequate overlap of histograms at these temperatures. Features corresponding to the characteristic isomerization (around 400 K) and the

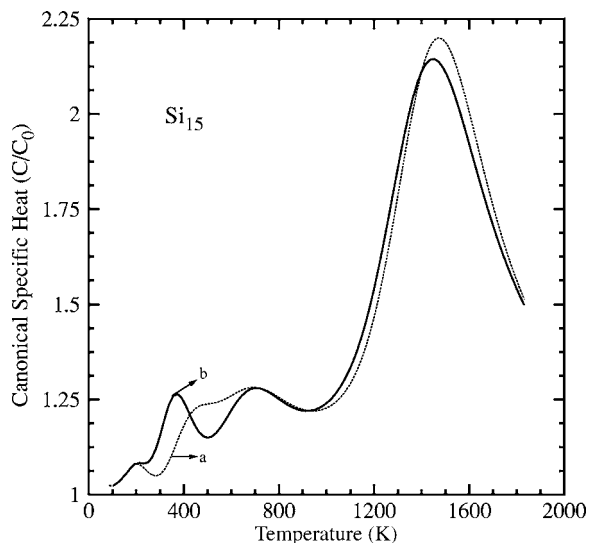


FIG. 14. Normalized canonical heat capacity of Si_{15} with two different sets of temperatures.

solidlike-to-liquidlike transition (around 800 K) merge, leading to an incomplete picture of finite-temperature behavior. However, a more complete picture is obtained from the heat-capacity curve (*b*). We have ensured that curve (*b*) does not change with the addition of further temperatures.

IV. CONCLUSIONS

We have presented the thermodynamics of small silicon and tin clusters (Si_{10} , Si_{15} , Si_{20} , Sn_{10} , and Sn_{20}) within the LDA and the GGA. The finite-temperature behavior of Si_{10} and Sn_{10} is dominated by isomerization processes. These clusters fragment around 2800 and 2600 K, respectively. The main peak in the heat capacity corresponds to the observed fragmentation rather than to a solidlike-to-liquidlike transition. The similarities observed in the finite-temperature behavior of these two clusters suggest a strong influence of the ground-state structures on their finite-temperature behavior. Si_{15} fragments around 1800 K; however, it exhibits a liquid-

like behavior over a short temperature range (900 to 1400 K) before fragmenting. The considerably lower fragmentation temperature of Si_{15} as compared to Si_{10} is attributed to the separation of the TTP unit from rest of the atoms. In contrast, the fragmentation of Si_{10} is associated with the breaking of the highly stable TTP unit. Si_{20} and Sn_{20} are found to dissociate without melting around 1200 and 650 K, respectively. Our simulations are in agreement with the available experimental data.

ACKNOWLEDGMENTS

We are grateful to Professor K. A. Jackson for providing us with the ground-state configuration of Si_{20} . C-DAC (Pune) is acknowledged for providing us with supercomputing facilities. The authors thank Indo French Centre For Promotion Of Advanced Research (IFCPAR) for partial financial support.

-
- ¹M. Schmidt, R. Kusche, B. von Issendorff, and H. Haberland, *Nature (London)* **393**, 238 (1998); M. Schmidt and H. Haberland, *C. R. Phys.* **3**, 327 (2002); H. Haberland, T. Hippler, J. Donges, O. Kostko, M. Schmidt and B. von Issendorff, *Phys. Rev. Lett.* **94**, 035701 (2005).
- ²A. A. Shvartsburg and M. F. Jarrold, *Phys. Rev. Lett.* **85**, 2530 (2000).
- ³G. A. Breaux, R. C. Benirschke, T. Sugai, B. S. Kinnear, and M. F. Jarrold, *Phys. Rev. Lett.* **91**, 215508 (2003).
- ⁴G. A. Breaux, D. A. Hillman, C. M. Neal, R. C. Benirschke, and M. F. Jarrold, *J. Am. Chem. Soc.* **126**, 8628 (2004).
- ⁵G. A. Breaux, C. M. Neal, B. Cao, and M. F. Jarrold, *Phys. Rev. Lett.* **94**, 173401 (2005).
- ⁶Z. Y. Lu, C. Z. Wang, and K. M. Ho, *Phys. Rev. B* **61**, 2329 (2000).
- ⁷A. Vichare, D. G. Kanhere, and S. A. Blundell, *Phys. Rev. B* **64**, 045408 (2001).
- ⁸K. Joshi, D. G. Kanhere, and S. A. Blundell, *Phys. Rev. B* **66**, 155329 (2002).
- ⁹K. Joshi, D. G. Kanhere, and S. A. Blundell, *Phys. Rev. B* **67**, 235413 (2003).
- ¹⁰S. Chacko, Kavita Joshi, D. G. Kanhere, and S. A. Blundell, *Phys. Rev. Lett.* **92**, 135506 (2004).
- ¹¹M. Manninen, A. Rytönen, and M. Manninen, *Eur. J. Phys.* **29**, 39 (2004).
- ¹²F. C. Chuang, C. Z. Wang, S. Ogut, J. R. Chelikowsky, and K. M. Ho, *Phys. Rev. B* **69**, 165408 (2004).
- ¹³S. Chacko, D. G. Kanhere, and S. A. Blundell, *Phys. Rev. B* **71**, 155407 (2005).
- ¹⁴K. Fuke, K. Tsukamoto, F. Misaizu, and M. Sanekata, *J. Chem. Phys.* **99**, 7807 (1993).
- ¹⁵A. A. Shvartsburg, M. F. Jarrold, B. Liu, Z. Y. Lu, C. Z. Wang and K.-M. Ho, *Phys. Rev. Lett.* **81**, 4616 (1998).
- ¹⁶K.-M. Ho, A. A. Shvartsburg, B. Pan, Z. Y. Lu, C. Z. Wang, J. G. Wacker, J. L. Fye, and M. F. Jarrold, *Nature (London)* **392**, 582 (1998).
- ¹⁷B. Liu, Z. Y. Lu, B. Pan, C. Z. Wang, K. M. Ho, A. A. Shvartsburg, and M. F. Jarrold, *J. Chem. Phys.* **109**, 9401 (1998).
- ¹⁸K. Zickfeld, M. E. Garcia, and K. H. Bennemann, *Phys. Rev. B* **59**, 13422 (1999).
- ¹⁹A. A. Shvartsburg and M. F. Jarrold, *Chem. Phys. Lett.* **317**, 615 (2000).
- ²⁰J. Muller, B. Liu, A. A. Shavartsburg, S. Ogut, J. R. Chelikowsky, K. W. Michael Sui, K.-M. Ho, and G. Gantefor, *Phys. Rev. Lett.* **85**, 1666 (2000).
- ²¹L. Mitás, J. C. Grossman, I. Stich, and J. Tobik, *Phys. Rev. Lett.* **84**, 1479 (2000).
- ²²I. Rata, A. A. Shvartsburg, M. Horoi, T. Frauenheim, K. W. Michael Siu, and K. A. Jackson, *Phys. Rev. Lett.* **85**, 546 (2000).
- ²³A. D. Zdetsis, *Phys. Rev. A* **64**, 023202 (2001).
- ²⁴A. A. Shvartsburg, R. R. Hudgins, P. Dugourd, and M. F. Jarrold, *Chem. Soc. Rev.* **30**, 36 (2001).
- ²⁵B. K. Panda, S. Mukherjee, and S. N. Behera, *Phys. Rev. B* **63**, 045404 (2001).
- ²⁶K. A. Jackson, M. Horoi, I. Chaudhuri, T. Frauenheim, and A. A. Shvartsburg, *Phys. Rev. Lett.* **93**, 013401 (2003).
- ²⁷Q. Sun, Q. Wang, P. Jena, S. Waterman, and Y. Kawazoe, *Phys. Rev. A* **67**, 063201 (2003).
- ²⁸X. L. Zhu and X. C. Zeng, *J. Chem. Phys.* **118**, 3558 (2003).
- ²⁹X. L. Zhu, X. C. Zeng, and B. Pan, *J. Chem. Phys.* **120**, 8985 (2004).
- ³⁰S. Yoo and X. C. Zeng, *Angew. Chem., Int. Ed.* **44**, 1491 (2005).
- ³¹Y. Tai, J. Murakami, C. Majumdar, V. Kumar, H. Mizuseki, and Y. Kawazoe, *J. Chem. Phys.* **117**, 4317 (2002).
- ³²Y. Tai, J. Murakami, C. Majumdar, V. Kumar, H. Mizuseki, and Y. Kawazoe, *Eur. Phys. J. D* **24**, 295 (2003).
- ³³Y. Tai and J. Murakami, *Chem. Phys. Lett.* **339**, 9 (2001).
- ³⁴A. L. Zhang, Y. Liu, R. F. Curl, F. K. Tittel, and R. E. Smalley, *J. Chem. Phys.* **88**, 1670 (1988).
- ³⁵G. A. Breaux, C. M. Neal, B. Cao, and M. F. Jarrold, *Phys. Rev. B* **71**, 073410 (2005).

- ³⁶A. A. Shvartsburg and M. F. Jarrold, Phys. Rev. A **60**, 1235 (1999).
- ³⁷M. C. Payne, M. P. Teter, D. C. Allen, T. A. Arias, and J. D. Joannopoulos, Rev. Mod. Phys. **64**, 1045 (1992).
- ³⁸D. Vanderbilt, Phys. Rev. B **41**, R7892 (1990).
- ³⁹*Vienna ab initio simulation package* (Technische Universität Wien, 1999); G. Kresse and J. Furthmüller, Phys. Rev. B **54**, 11169 (1996).
- ⁴⁰B. Silvi and A. Savin, Nature (London) **371**, 683 (1994).
- ⁴¹S. Nosé, Prog. Theor. Phys. **103**, 1 (1991).
- ⁴²D. J. Evans and G. P. Morriss, *Statistical Mechanics of Non-Equilibrium Liquids* (Academic Press, London, 1990).
- ⁴³A. M. Ferrenberg and R. H. Swendsen, Phys. Rev. Lett. **61**, 2635 (1988); P. Labastie and R. L. Whetten, *ibid.* **65**, 1567 (1990).
- ⁴⁴D. G. Kanhere, A. Vichare, and S. A. Blundell, in *Reviews in Modern Quantum Chemistry*, edited by K. D. Sen (World Scientific, Singapore, 2001).
- ⁴⁵K. Raghavachari and C. M. Rohlfing, J. Chem. Phys. **89**, 2219 (1988); P. Ballone, W. Andreoni, R. Car, and M. Parrinello, Phys. Rev. Lett. **60**, 271 (1988); C. M. Rohlfing and K. Raghavachari, Chem. Phys. Lett. **167**, 559 (1990).